



**HAL**  
open science

## Factors Affecting the Population of Excited Charge Transfer States in Adenine/Guanine Dinucleotides: A Joint Computational and Transient Absorption Study

Vasilis Petropoulos, Lara Martinez-Fernandez, Lorenzo Uboldi, Margherita Maiuri, Giulio Cerullo, Evangelos Balanikas, Dimitra Markovitsi

### ► To cite this version:

Vasilis Petropoulos, Lara Martinez-Fernandez, Lorenzo Uboldi, Margherita Maiuri, Giulio Cerullo, et al.. Factors Affecting the Population of Excited Charge Transfer States in Adenine/Guanine Dinucleotides: A Joint Computational and Transient Absorption Study. *Biomolecules*, 2024, 14 (12), pp.1548. 10.3390/biom14121548 . hal-04829820

**HAL Id: hal-04829820**

**<https://cnrs.hal.science/hal-04829820v1>**

Submitted on 10 Dec 2024

**HAL** is a multi-disciplinary open access archive for the deposit and dissemination of scientific research documents, whether they are published or not. The documents may come from teaching and research institutions in France or abroad, or from public or private research centers.


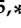



L'archive ouverte pluridisciplinaire **HAL**, est destinée au dépôt et à la diffusion de documents scientifiques de niveau recherche, publiés ou non, émanant des établissements d'enseignement et de recherche français ou étrangers, des laboratoires publics ou privés.



Distributed under a Creative Commons Attribution 4.0 International License

## Article

# Factors Affecting the Population of Excited Charge Transfer States in Adenine/Guanine Dinucleotides: A Joint Computational and Transient Absorption Study

Vasilis Petropoulos <sup>1</sup>, Lara Martinez-Fernandez <sup>2,\*</sup>, Lorenzo Uboldi <sup>1</sup>, Margherita Maiuri <sup>1</sup>, Giulio Cerullo <sup>1,3,\*</sup>, Evangelos Balanikas <sup>4</sup> and Dimitra Markovitsi <sup>5,\*</sup>

<sup>1</sup> Dipartimento di Fisica, Politecnico di Milano, Piazza Leonardo da Vinci 32, 20133 Milano, Italy; lorenzo.uboldi@polimi.it (L.U.)

<sup>2</sup> Departamento de Química Física de Materiales, Instituto de Química Física Blas Cabrera, Consejo Superior de Investigaciones Científicas, Calle Serrano 119, 28006 Madrid, Spain

<sup>3</sup> Istituto di Fotonica e Nanotecnologie-CNR, Piazza Leonardo da Vinci 32, 20133 Milano, Italy

<sup>4</sup> Laboratoire d'Optique et Biosciences, Ecole Polytechnique, CNRS—INSERM, Institut Polytechnique de Paris, 91120 Palaiseau, France

<sup>5</sup> Institut de Chimie Physique, CNRS-UMR8000, Université Paris-Saclay, 91405 Orsay, France

\* Correspondence: lmartinez@iqf.csic.es (L.M.-F.); giulio.cerullo@polimi.it (G.C.); dimitra.markovitsi@universite-paris-saclay.fr (D.M.)

**Abstract:** There is compelling evidence that the absorption of low-energy UV radiation directly by DNA in solution generates guanine radicals with quantum yields that are strongly dependent on the secondary structure. Key players in this unexpected phenomenon are the photo-induced charge transfer (CT) states, in which an electric charge has been transferred from one nucleobase to another. The present work examines the factors affecting the population of these states during electronic relaxation. It focuses on two dinucleotides with opposite orientation: 5'-dApdG-3' (AG) and 5'-dGpdA-3' (GA). Quantum chemistry calculations determine their ground state geometry and the associated Franck–Condon states, map their relaxation pathways leading to excited state minima, and compute their absorption spectra. It has been shown that the most stable conformer is *anti-syn* for AG and *anti-anti* for GA. The ground state geometry governs both the excited states populated upon UV photon absorption and the type of excited state minima reached during their relaxation. Their fingerprints are detected in the transient absorption spectra recorded with excitation at 266 nm and a time resolution of 30 fs. Our measurements reveal that in the large majority of dinucleotides, chromophore coupling is already operative in the ground state and that the charge transfer process occurs within ~120 fs. The competition among various relaxation pathways affects the quantum yields of the CT state formation in each dinucleotide, which are estimated to be 0.18 and 0.32 for AG and GA, respectively.

**Keywords:** DNA; dinucleotides; G-quadruplexes; polarity; directionality; charge transfer states; oxidative damage; photoionization; quantum yield; transient absorption spectroscopy; quantum chemistry



**Citation:** Petropoulos, V.; Martinez-Fernandez, L.; Uboldi, L.; Maiuri, M.; Cerullo, G.; Balanikas, E.; Markovitsi, D. Factors Affecting the Population of Excited Charge Transfer States in Adenine/Guanine Dinucleotides: A Joint Computational and Transient Absorption Study. *Biomolecules* **2024**, *14*, 1548. <https://doi.org/10.3390/biom14121548>

Academic Editors: Marino J. E. Resendiz, Chryssostomos Chatgililoglu and Yuan Liu

Received: 11 October 2024  
Revised: 15 November 2024  
Accepted: 27 November 2024  
Published: 3 December 2024



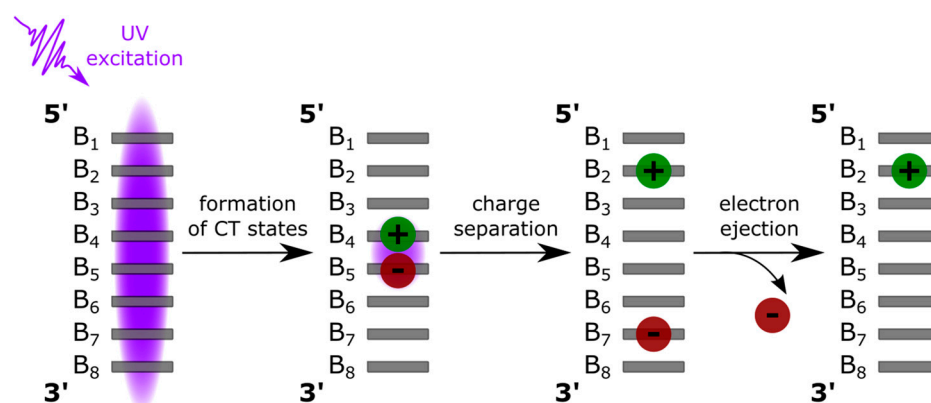
**Copyright:** © 2024 by the authors. Licensee MDPI, Basel, Switzerland. This article is an open access article distributed under the terms and conditions of the Creative Commons Attribution (CC BY) license (<https://creativecommons.org/licenses/by/4.0/>).

## 1. Introduction

Guanine radical cations, which are precursors to oxidative DNA damage, may be generated through an ionization process triggered by ion beams or electromagnetic radiation [1]. Regarding photoionization, it was long considered to be limited at wavelengths shorter than 210 nm [2–4]. However, during the past two decades, it has been clearly observed that DNA in aqueous solution also undergoes one-photon ionization at much longer wavelengths [5], extending to the UVB spectral domain [6]. The photoionization quantum yields ( $\Phi_i$ ) at low energies are much smaller than those at high energies [7]. For example, the  $\Phi_i$  determined for calf thymus DNA is  $\sim 50 \times 10^{-3}$  [4,8] at 193 nm and only

$2 \times 10^{-3}$  at 266 nm [5]. Yet, the latter value is similar to the quantum yield determined at 254 nm for the totality of pyrimidine dimers [9], which are considered the major lesions provoked in DNA by direct absorption of UV radiation [10]. Therefore, the mechanism underlying the low-energy photoionization deserves further investigation.

The picture emerging from the ensemble of studies is that in low-energy photoionization, the electron is not ejected vertically, without prior geometrical rearrangement of the system, as in the case of the high-energy process [11–13]. Instead, photoionization is the result of a multistep mechanism, which is strongly correlated with the relaxation of the DNA electronic excited states (Figure 1). The Franck–Condon states, mostly extending over more than one nucleobase, may evolve toward excited charge transfer (CT) states [14–23]. In the latter, an electron is transferred between two stacked nucleobases, the driving force being the difference between their oxidation potentials, which are modulated by the local environment. A small fraction of CT states undergoes charge separation, which is a process that has already been reported in the literature [24,25]. Finally, an electron is ejected from the nucleobase bearing the negative charge because its ionization potential is lower compared to its neutral counterpart [26]. Thus, it is understandable why the low-energy photoionization strongly depends on the secondary DNA structure; it is not detectable for its monomeric building blocks, dinucleotides, or poorly stacked single strands ( $\Phi_i < 3 \times 10^{-4}$ ), and  $\Phi_i$  increases to  $1\text{--}2 \times 10^{-3}$  for duplexes and up to  $15 \times 10^{-3}$  for guanine quadruplexes (G-quadruplexes) [5,27].



**Figure 1.** Successive steps potentially leading to DNA photoionization at low energies.  $B_i$  designates stacked nucleobases.

Thanks to the structural versatility of G-quadruplexes, it was shown that, among other factors, such as the nature of the metal cation in their central cavity,  $\Phi_i$  depends on the polarity (also called directionality) of the DNA strands [27], that is the order in which nucleobases are connected via the backbone from the 5' end to the 3' end. Those determined for a series of structures composed of four identical 5'-XGGGG-3' or 5'-GGGGX-3' strands and characterized by the presence of ending groups X, [X = adenine (A) or thymine (T)] at one end, are presented on Table 1. The nearly threefold variation observed in the  $\Phi_i$  values was correlated with the formation of CT states between the ending group X and guanine of the quadruplex core,  $G^+ \rightarrow X^-$ ; the directionality of the transfer is determined by the fact that G is the nucleobase with the lowest oxidation potential [28]. The lifetimes of the CT states ( $\tau_{CT}$ ), that is, the time required for charge recombination leading back to the ground state, are also presented in Table 1. They were determined for the corresponding dinucleoside monophosphates, 5'-dXpG-d3' and or 5'-dGpdX-3', which, for simplicity, are hereafter called dinucleotides and abbreviated as XG and GX, respectively. We remark that, indeed, the longer the lifetime, the higher the  $\Phi_i$  value. This is in line with the mechanism depicted in Figure 1; a longer lifetime is expected to favor charge separation under the effect of conformational motions. Yet, the correlation is not linear, indicating that other factors also play an important role.

**Table 1.** Correlation between the  $\Phi_i$  values determined for tetramolecular G-quadruplexes composed of four identical strands 5'-XGGGG-3'/5'-GGGGX-3' (X = adenine, thymine) and the lifetimes of the CT states ( $\tau_{CT}$ ) in GX and XG dinucleotides; excitation wavelength: 266 nm.

G-Quadruplex <sup>1</sup>	$\Phi_i \times 10^3$ [27]	Dinucleotide <sup>2</sup>	$\tau_{CT}$ (ps)
4 × (5'-GGGGA-3')	12.6 ± 0.1	GA	170 ± 10 [29]
4 × (5'-AGGGG-3')	9.9 ± 0.4	AG	112 ± 12 [29]
4 × (5'-GGGGT-3')	8.8 ± 0.2	GT	13 ± 1 [30]
4 × (5'-TGGGG-3')	4.7 ± 0.7	TG	5.44 ± 0.03 [31]

<sup>1</sup> From ns TA experiments; <sup>2</sup> from fs TA experiments.

The objective of the present work is to explore the structural and electronic factors that affect the population of CT states in the dinucleotides AG and GA. This is a necessary step before tackling the more complex four-stranded structures, in which different types of CT states may be formed [32,33]. Our comparative study is conducted using quantum chemistry calculations and broadband ultrafast transient absorption spectroscopy as the main tools. Previous publications have reported lifetimes of CT states in these systems and estimated quantum yields ( $\Phi_{CT}$ ) for their formation (Table 2). Despite the existing studies, several questions remain open. The first point concerns the stacking pattern characterizing each dinucleotide. This question was either eluded [34] or it was implicitly considered that the geometry corresponds to the conformation adopted in B-form double helices [29,35], which is determined by interactions involving the ensemble of the duplex structure. Secondly, it was considered that electronic excitations in all the stacked configurations give rise to a CT state;  $\Phi_{CT}$  was determined from the recovery of the ground state bleaching signal in transient absorption (TA) experiments [34]. In the meantime, quantum chemistry calculations revealed the existence of various Franck–Condon transitions in each dinucleotide, which may evolve toward different minima [29,31]. Moreover, quantum dynamical simulations showed that the probability of populating a CT state in CG steps is lower compared to that of GC steps (C = cytosine) [36]. Finally, it was estimated that the formation of the CT state in AG takes 5–10 ps; the latter conclusion was drawn from experiments whose time resolution was 150 fs after deconvolution using global analysis with multi-exponential functions [35]. However, in our recent study on the dinucleotide TG, which was performed with a time resolution of 30 fs, we showed that this process is much faster, occurring within 100 fs [31].

**Table 2.** Lifetimes (in ps) of the CT states in AG and GA dinucleotides reported in the literature; in parentheses: excitation/probed wavelengths or energies.

AG	GA
105 ± 30 (267 nm/252 nm) <sup>1</sup> [34]	-
124 ± 4 (260 nm/330–680 nm) <sup>2</sup> [35]	-
280 ± 160 (266 nm/1500–1700 cm <sup>-1</sup> ) <sup>3</sup> [37]	420 ± 120 (266 nm/1500–1700 cm <sup>-1</sup> ) <sup>4</sup> [37]
112 ± 12 (266 nm/330–680 nm) [29]	170 ± 10 (266 nm/500–645 nm) [29]

$\Phi_{CT}$ : <sup>1</sup> 33 ± 6%; <sup>2</sup> >26%; <sup>3</sup> 32 ± 15%; <sup>4</sup> 42 ± 20%.

In order to elucidate the above points, in the present study, we follow the methodology we developed recently using TG as the showcase [31]. Transient absorption spectra (TAS) are recorded from 20 fs to 40 ps over the 330–650 nm range with a temporal resolution of ~30 fs. In parallel, quantum chemistry calculations determine the associated Franck–Condon states of the most stable conformers with stacked nucleobases and map their relaxation along the potential energy surfaces (PES); they also provide computed TAS for both the Franck–Condon states and the PES minima, facilitating their identification in the experimental data. Our work reveals the competition among various relaxation pathways, depending on the ground state geometry and the excitation wavelength, which affect  $\Phi_{CT}$ .

## 2. Materials and Methods

### 2.1. Samples

**AG** and **GA** dinucleotides, which were purified by desalting and, subsequently, using reverse phase HPLC, were purchased by Eurogentec (Liege/Belgium). The corresponding MALDI-TOF spectra, which are shown in Figure S1 in the Supplementary Materials (SM), indicate that both impurities and monomeric constituents have been efficiently removed. We note that electron paramagnetic resonance measurements detected other contaminants in commercially available oligonucleotides [38]. Moreover, the presence of monomeric chromophores in the solution may lead to an erroneous interpretation of the experimental results because signals originating from such “monomer impurities” are attributed to unstacked nucleobases of nucleotides. The dinucleotides were dissolved in phosphate buffer ( $0.12 \text{ molL}^{-1}$ , pH 7.0) using Milli-Q water. Their concentration ( $4 \times 10^{-3} \text{ molL}^{-1}$ ) was much higher than that of absorbed photons ( $8 \times 10^{-6} \text{ molL}^{-1}$ ), rendering two-photon absorption highly improbable. Experiments on the monomeric chromophores were performed using the mononucleosides 2'-deoxyadenosine (dA) and 2'-deoxyguanosine (dG) in water, instead of the corresponding mononucleotides, which have a great propensity to aggregate in solutions containing salts [39]. All measurements were performed at room temperature.

### 2.2. Spectroscopic Setups

Steady-state absorption spectra were recorded by means of a PerkinElmer Lambda 1050 Spectrophotometer, manufactured by PerkinElmer Inc., Waltham, MA, USA, utilizing quartz cells with a 1 mm path length. Circular dichroism (CD) spectra were obtained on a JASCO J-815 CD Spectrometer, produced by JASCO Corporation, Tokyo, Japan, using 0.2 mm quartz cuvettes.

TA experiments were conducted using an amplified Ti:Sapphire laser, Libra, Coherent, sourced from Santa Clara, CA, USA (800 nm, 100 fs pulse duration, 1 kHz repetition rate) [40]. Initially, a portion of the laser beam was frequency-doubled to drive a non-collinear optical parametric amplifier (NOPA), generating broadband visible pulses. These pulses were then compressed using chirped dielectric mirrors. Subsequently, the compressed pulses were frequency-doubled in a 20  $\mu\text{m}$ -thick  $\beta$ -barium borate crystal to create broadband UV pump pulses that were tunable across the 250–300 nm range. The UV pump pulses were characterized by two-dimensional spectral interferometry and compressed to 24 fs (FWHM) with the aid of a prism pair before being tuned to 266 nm for the experiment. To generate broadband probe pulses, a portion of the primary laser beam was focused onto a 2 mm-thick  $\text{CaF}_2$  plate, producing a white light continuum that spanned from 330 nm to 650 nm. The pump and probe pulses were then non-collinearly focused onto the sample, with spot sizes of 180  $\mu\text{m}$  and 95  $\mu\text{m}$ , respectively. Their relative polarizations were adjusted to the magic angle ( $54.7^\circ$ ). The pump fluence was maintained at  $100 \mu\text{J cm}^{-2}$ , ensuring that the differential absorption (DA) signals remained below  $10^{-3}$ . This approach effectively minimized contributions from coherent processes and solvated electrons resulting from the two-photon ionization of the solvent. To avoid photodamage during the experiment, a 6 mL solution was continuously circulated through a 1 mm-thick quartz cell using a peristaltic pump. Details on the determination of the time resolution are given in reference [31].

### 2.3. Computational Techniques

Quantum mechanical (QM) calculations were based on the density functional theory (DFT), and its time-dependent (TD-DFT) version, using the M052X functional [41,42], the 6–31G(d) basis set, and an implicit polarizable continuum model (PCM) [43] for solvent. One  $\text{Na}^+$  ion was considered per dinucleotide. This method is known to provide accurate results when optimizing charged species and computing spectral properties and PES in small DNA models, as well as in G-quadruplexes [20,33,44,45].

The vertical absorption energies, intensities (oscillator and rotatory strengths) of the different excited states, and corresponding PES were characterized using the above-described methodologies, but resorting to TD-DFT. The CT character was computed using a

simple Mulliken population analysis in terms of  $\delta q$ , i.e., the difference between the charges in the excited state and the ground state. All these calculations were performed with the Gaussian16 program [46].

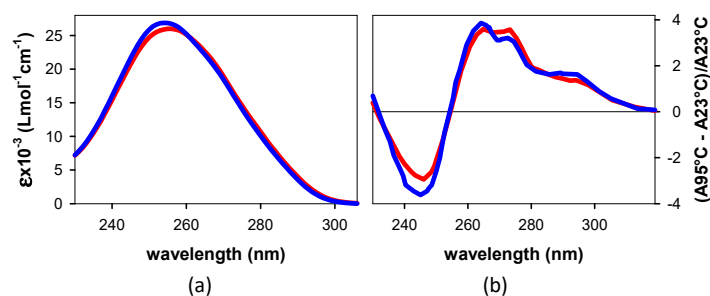
The computed spectra are compared with the experimental spectra after shifting their energy by  $-0.65$  eV. Part of this difference arises from the absence of vibronic effects in our computations [47]. The value of  $-0.65$  eV was chosen so that the energy computed for the lowest bright state (La) of dG in water and the corresponding value derived from deconvolution of the experimental spectrum (Figure 2 in reference [48]) coincide. A multifunctional analyzer (multiwfn program) [49] provided the transition dipole moments between the excited states for the computation of the TAS, for which there is no reference regarding the appropriate shift; therefore, for the sake of uniformity, we shifted them in the same way as for the steady-state spectra. In all cases, a phenomenological broadening via a Gaussian function with a width of  $0.4$  eV (FWHM) was applied to each transition.

### 3. Results

#### 3.1. Experimental

##### 3.1.1. Steady-State Spectroscopy

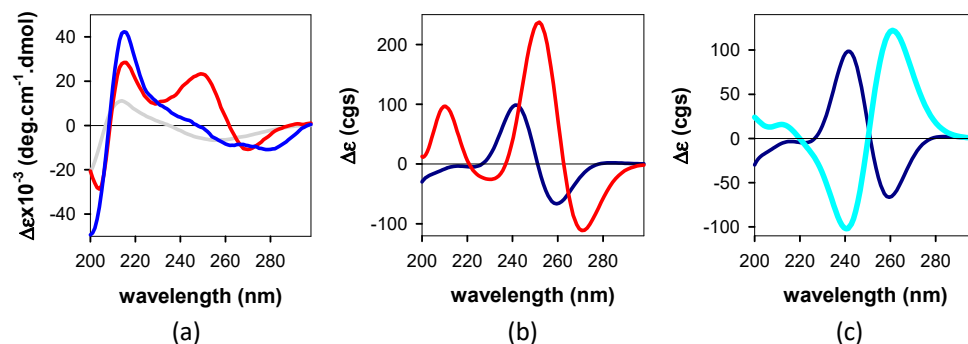
The steady-state absorption spectra of the studied dinucleotides are plotted in Figure 2a, taking into account the molar absorption coefficients ( $\epsilon$ ) provided by Eurogentec. Although they seem very similar, subtle differences can be observed; the spectrum of AG peaks at  $254$  nm, and its maximum intensity is slightly higher than that of GA, which peaks at  $256$  nm. The same similarity is observed for the thermal absorption spectra (Figure 2b), which are determined from the difference between the spectra recorded at  $95$  °C, where stacking is destroyed, and those recorded at  $23$  °C. Both spectra reveal a hypochromic effect above  $255$  nm at room temperature, reaching  $3.7 \pm 0.1\%$ , and a hyperchromic effect at shorter wavelengths.



**Figure 2.** (a) Steady-state and (b) thermal absorption spectra determined for AG (blue) and GA (red). The thermal spectra are the difference between the steady-state absorption spectra recorded for each dinucleotide at  $95$  °C ( $A_{95}$  °C) and  $23$  °C ( $A_{23}$  °C), divided by  $A_{23}$  °C.

An important difference in the interchromophore interactions within each dinucleotide is attested by the CD spectra shown in Figure 3a. The dinucleotide spectra differ from the spectrum recorded for an equivalent mixture of mononucleotides, i.e., having the same concentration of dA and dG as the dinucleotide. The CD spectrum of GA is characterized by well-defined positive (at  $215$  and  $249$  nm) and negative (at  $204$  and  $270$  nm) peaks. While the positive peak at  $215$  nm, which is preceded by a negative feature at short wavelengths, is also present in the CD spectrum of AG, its structure above  $220$  nm is ill-defined, presenting multiple local fluctuations.

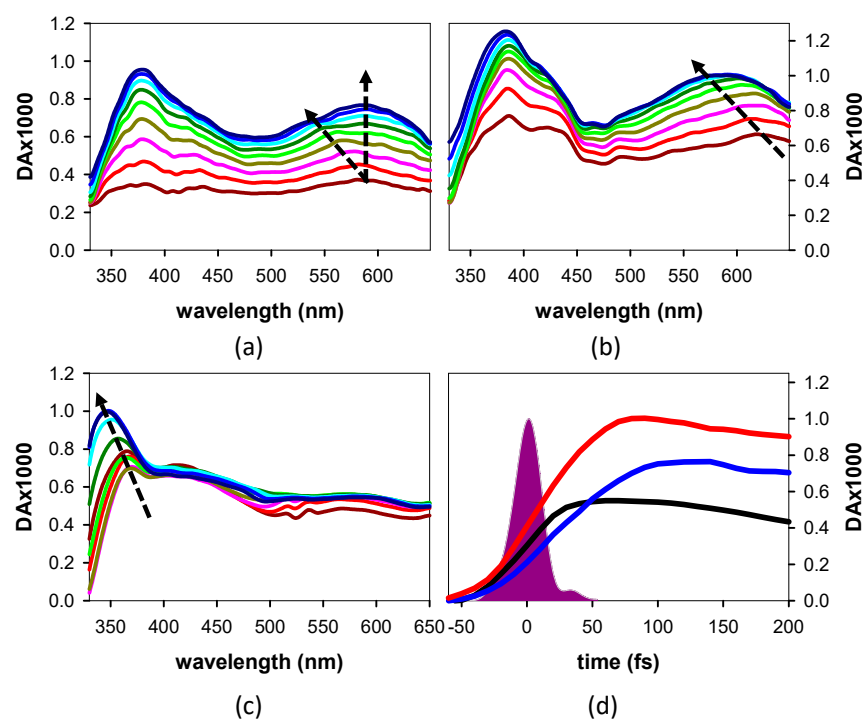




**Figure 3.** CD spectra recorded for **AG** (blue), **GA** (red), and an equimolar mixture of dA and dG (gray) (a) and computed for *anti-syn AG* (dark blue), *anti-anti GA* (red), and *anti-anti AG* (cyan) (b,c).

### 3.1.2. Time-Resolved Spectroscopy

The experimental *TAS* recorded from 20 fs to 100 fs for **AG**, **GA**, and an equivalent mixture of dA and dG are presented in Figure 4a–c, respectively.



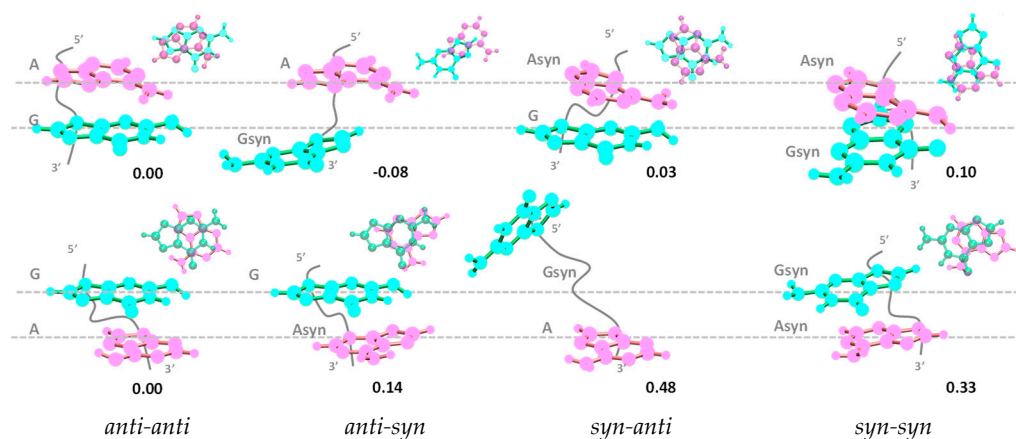
**Figure 4.** Experimental *TAS* obtained for **AG** (a), **GA** (b), and an equivalent mixture of dA and dG (c) recorded between 20 fs (dark red) and 100 fs (dark blue) with 10 fs steps. *TA* signals at 600 nm obtained for **AG** (blue), **GA** (red), and an equivalent mixture of dA and dG (black) (d).

The most notable feature in the evolution of the dinucleotide *TAS* is their increase in intensity over the probed spectral region. Much smaller variations are observed in the case of monomeric chromophores; the largest changes, appearing below 380 nm, are absent from the dinucleotide *TAS*. The rise in the mononucleosides' *TA* signal at 600 nm (Figure 4d) stops at the end of the laser pulse. In contrast, in the case of the dinucleotides, it is pursued for a few tens of fs more, reaching a maximum value at around 130 fs for **AG** and 110 for **GA**. After this time, a slow decay is observed, with concomitant changes in the spectral shapes, which have been reported in our previous publication on these systems [29].

### 3.2. Computational

#### 3.2.1. Ground State Geometry

We optimized the ground state geometries considering four possible stacking modes: *anti-anti*, *anti-syn*, *syn-anti*, and *syn-syn*, where *anti* and *syn* refer to the position of each nucleobase (in the order 5' to 3'), with respect to the angle of the glycosidic bond associated with the deoxyribose moiety. The resulting conformers are presented in Figure 5. The energies of the four conformers computed for each dinucleotide (Tables S1 and S2 in the Supplementary Materials (SM)) are given using as a reference that of the corresponding *anti-anti* conformer, which is the one encountered in B-form duplexes.



**Figure 5.** Side and top views of the ground state structures corresponding to the four possible conformers with stacked nucleobases computed for **AG** and **GA**. Their relative energies ( $\Delta G$ , in eV) are shown in black. Adenine and guanine are depicted in pink and turquoise, respectively, and the backbone is in gray. The top view of *syn-anti* **GA** has been omitted because the overlap is very poor.

The relative energy values reveal that the two systems do not behave in the same way. The most stable conformer of **AG** is *anti-syn*, while for **GA**, the minimum energy is found for the *anti-anti* conformer. A second important difference concerns the energy gap between the lowest and highest values: 0.18 eV for **AG** and nearly twice as high (0.33) for **GA**. Given that the energy of thermal fluctuations at room temperature amounts to 0.025 eV, the *anti-anti* conformer, whose energy differs by 0.14 eV from the next more stable one, is likely to be the dominant structure of the **GA** solution. In contrast, the *anti-syn* conformer could coexist in the **AG** solution with some percentage of the *anti-anti* conformer.

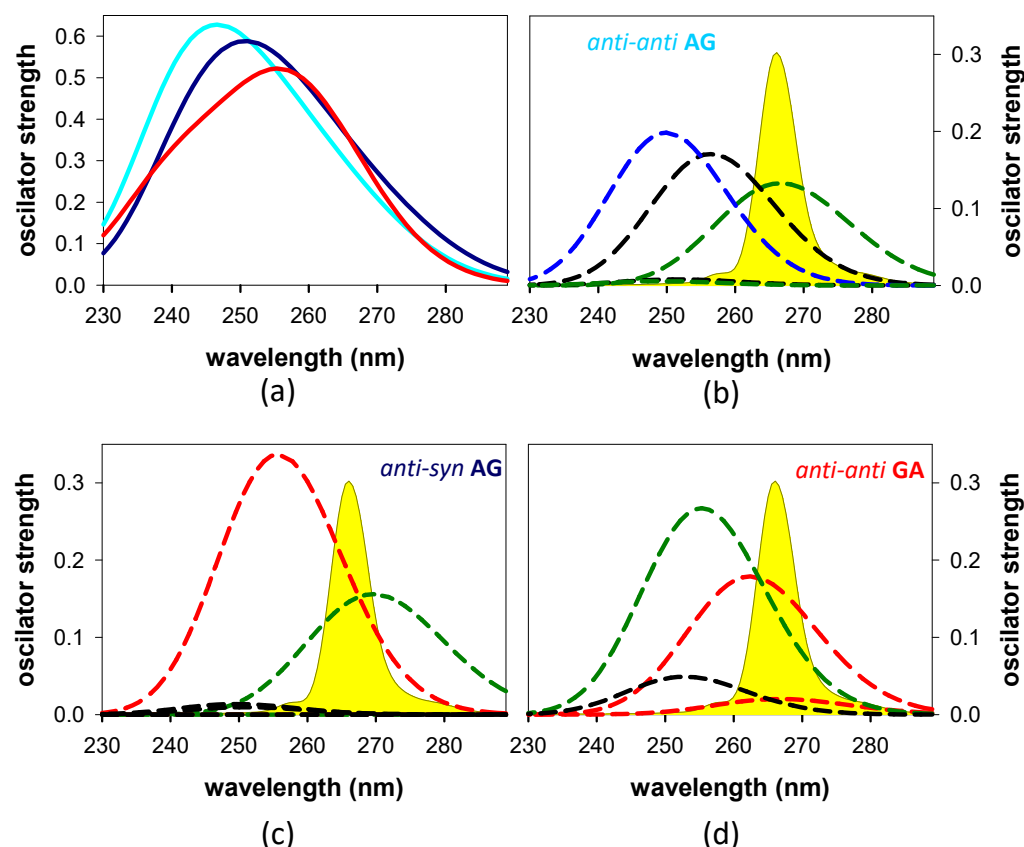
Figure 3b shows the CD spectra computed for the most stable conformers, *anti-syn* **AG** and *anti-anti* **GA**; starting from long wavelengths, both exhibit a negative peak, followed by a positive one. In contrast, the two conformers of **AG** exhibit quite opposite patterns (Figure 3c).

#### 3.2.2. Franck–Condon States and Their Evolution

In view of the abovementioned findings, we computed the properties of the excited states for *anti-syn* **AG**, *anti-anti* **AG**, and *anti-anti* **GA**. The Franck–Condon states of *anti-anti* **AG** and *anti-anti* **GA**, as well as the minima in their PES, were reported in reference [27]; their properties are also shown in the Supplementary Materials (SM), together with those of *anti-syn* **AG**, which were determined for the first time in the present study (Tables S3–S5).

Based on the abovementioned data, we calculated the steady-state absorption spectrum of each conformer and simulated those of the individual transitions that compose it (Figure 6). We observe in Figure 6a that for both **AG** conformers, the maximum is located at shorter wavelengths, and its intensity is higher than that of **GA**.





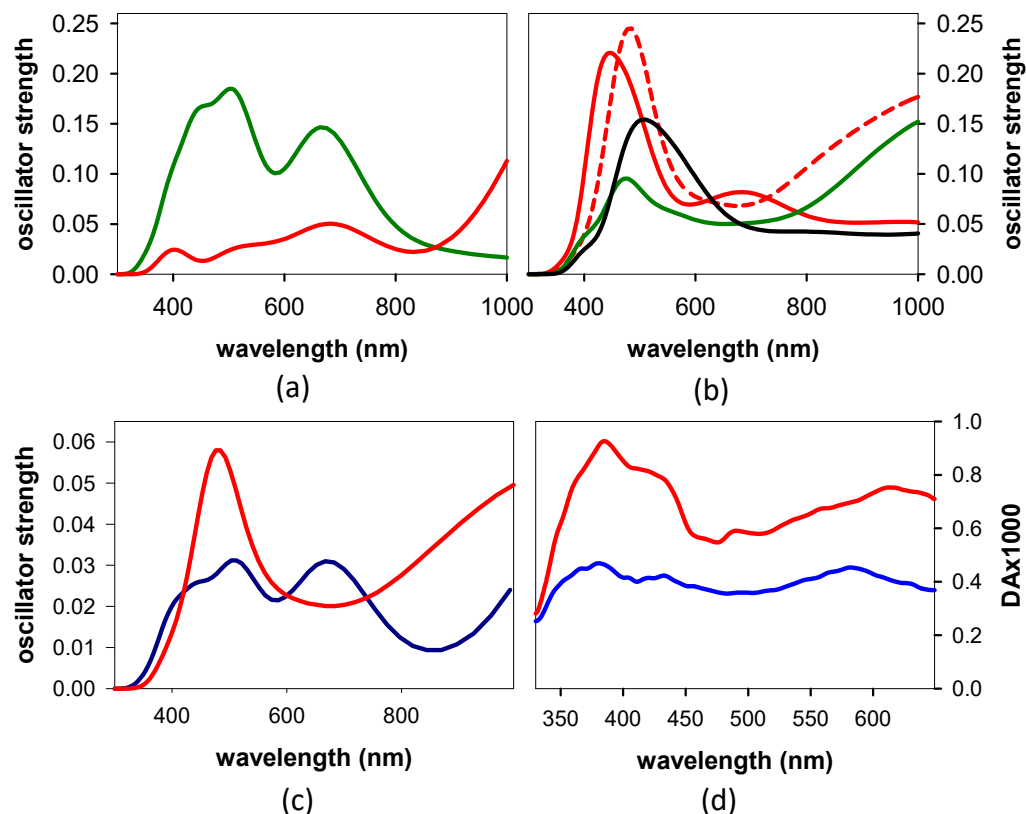
**Figure 6.** Steady-state absorption spectra (solid lines) computed for *anti-anti AG* (cyan), *anti-syn AG* (dark blue), and *anti-anti GA* (red) (a). Individual transitions (dashed lines, see Tables S3–S5 in the Supplementary Materials (SM)) composing each one of them (b–d); the color code of the dashed lines is defined by the minimum toward which evolves each individual transition (see Tables S6–S8 in the Supplementary Materials (SM)): min-CT (red); min- $\pi\pi^*G(L_a)$  (green); min- $n\pi^*A$  (black);  $\pi\pi^*$  exciton delocalized on A and G (blue). The spectrum of the exciting laser pulse is shown in yellow.

The main electronic states correlated with the steady-state absorption spectrum of *anti-anti AG* in the 240–300 nm region are  $\pi\pi^*G(L_a)$  ( $S_1$ ),  $\pi\pi^*A$  ( $S_2$ ), and  $G^+ \rightarrow A^- CT$  ( $S_4$ ) (Figure 6b, Table S3). Their evolution along the corresponding PES leads, respectively, to three different minima, min- $\pi\pi^*G(L_a)$ , min- $n\pi^*A$ , and min-exciton, i.e., a  $\pi\pi^*$  delocalized over A and G (Table S6). The same Franck–Condon states,  $\pi\pi^*G(L_a)$  ( $S_1$ ) and  $\pi\pi^*A$  ( $S_2$ ), are also present in the more stable *anti-syn AG* (Figure 6c, Table S4). Although  $S_1$  also evolves toward a min- $\pi\pi^*G(L_a)$  in this conformer,  $S_2$  reaches a minimum with a clear  $G^+ \rightarrow A^- CT$  character ( $\delta = 0.4$  a.u.) (Table S7). In the case of *anti-anti AG*, a min-CT is reached only following the population of the  $S_9$  state, which is located at 218 nm according to the scale adopted in Figure 6; thus, it is very unlikely to be populated by the exciting laser pulse used in our experiments, whose spectrum is also shown in Figure 6b–d.

Four electronic transitions, whose oscillator strength ranges from 0.020 to 0.267, underlie the absorption spectrum of *anti-anti GA* (Table S5 and Figure 6d) [27]. Two of them,  $S_1$  ( $\pi\pi^*G(L_a)$ ) and  $S_2$  ( $\pi\pi^*A$  combined to  $G^+ \rightarrow A^- CT$ ;  $\delta = 0.3$  a.u.), result in a min-CT ( $\delta = 0.7$  a.u.) (Table S8).  $S_3$ , whose main character is  $\pi\pi^*G(L_a)$ , with a small contribution of  $G^+ \rightarrow A^- CT$  ( $\delta = 0.1$  a.u.), results in min- $\pi\pi^*G(L_a)$ . Finally, the  $S_4$  state ( $n\pi^*A$ ) results in min- $n\pi^*A$ .

Next, we calculated the TAS of the Franck–Condon states for the most stable conformers of AG and GA (Figure 7c,d), more or less overlapping with the spectrum of the laser. We observe that both the shape and the oscillator strength differ from one state to the other and from one system to the other. All these states underlie the “global” TAS, but their contribution depends on the probability of being populated by the excitation pulse.

A rough estimate is obtained by multiplying each TAS by the oscillator strength of the corresponding steady-state transition at 266 nm (Figure 6c,d). The resulting linear combinations are shown in Figure 7c, where it appears that the intensity of the *anti-anti* GA TAS is significantly higher than that of *anti-syn* AG, in particular at the high- and low-energy sides.



**Figure 7.** TAS of Franck–Condon states. Computed for  $S_1$  (green) and  $S_2$  (red) of *anti-syn* AG (a) and  $S_1$  (red solid line),  $S_2$  (red dashed line),  $S_3$  (green), and  $S_4$  (black) of *anti-anti* GA (b); the color code is the same as that in Figure 6c,d. (c) Weighted sum of the TAS of all the states in Figure 6c (*anti-syn* AG: dark blue) and Figure 6d (red: *anti-anti* GA), each one scaled by the corresponding oscillator strength at 266 nm. (d) Experimental TAS recorded at 30 fs for AG (blue) and GA (red).

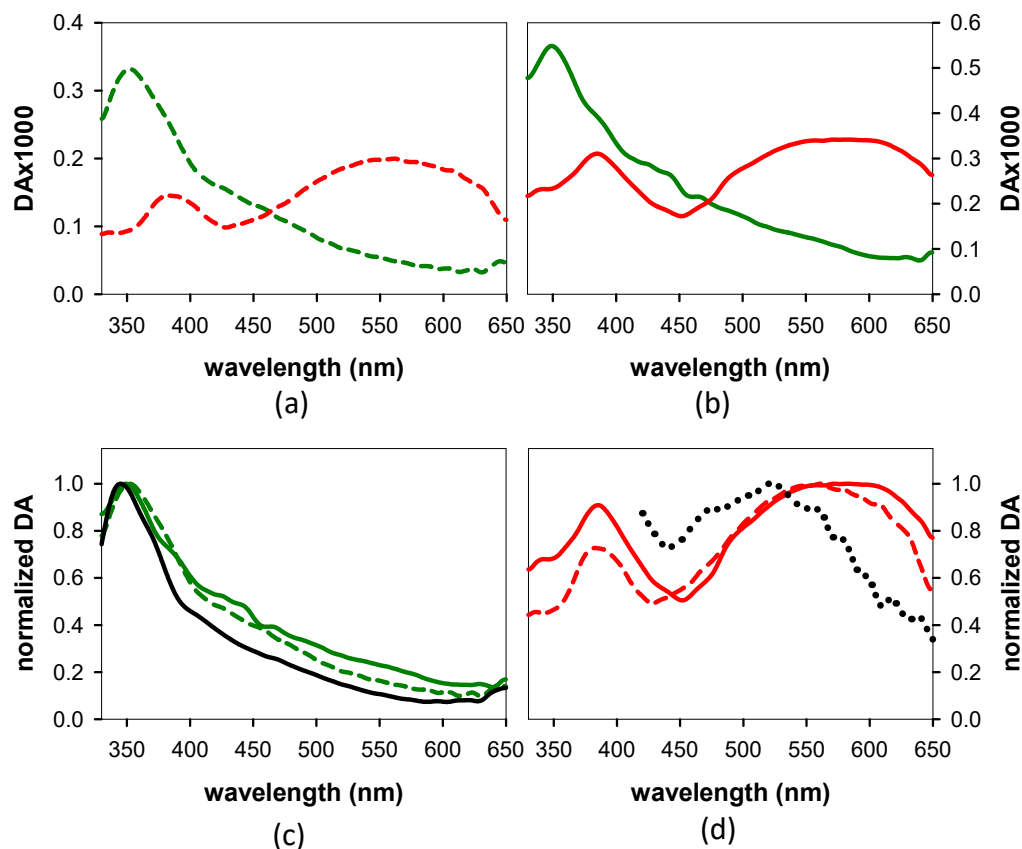
### 3.3. TAS of the Minima

From the computational results presented in the previous section, it appears that two main minima are expected to be populated during the excited state relaxation in the most stable conformers of AG and GA, *min-CT* and *min- $\pi\pi^*$ G(L<sub>a</sub>)*. The latter would also be reached from the less stable conformer, *anti-anti* AG, for which a third type of minimum, *min- $n\pi^*$ A* (Figure 6b), may also have a non-negligible contribution, as well as, to a lesser extent, a  $\pi\pi^*$  state delocalized on both A and G (exciton).

We searched the fingerprints of *min-CT* and *min- $\pi\pi^*$ G(L<sub>a</sub>)* in the experimental TAS. To this end, we performed a global analysis between 4 and 45 ps. We neglected the first 4 ps on purpose, so as to be sure that all the minima were reached and we could safely use exponential functions. As explained in detail in reference [31], if the abovementioned condition is not applied and numerous transient species coexist in the solution, the conclusions derived from such an analysis may be erroneous.

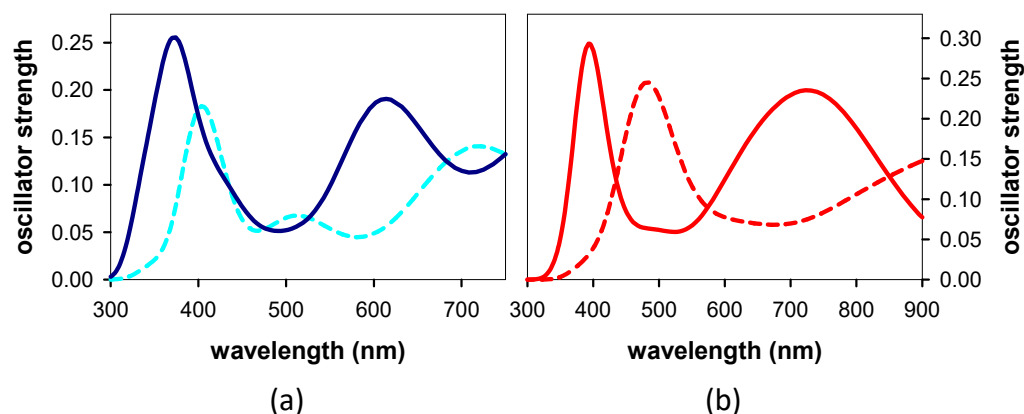
Decay-associated spectra (DAS) were derived using two exponential functions (Figure 8a,b). In order to minimize the number of variables, we fixed one of the time constants to the values determined previously from the TA decays measured between 500 and 645 nm by means of a different experimental setup [29]. In both cases, good-quality fits were obtained (Figure S2 in the Supplementary Materials (SM)). The spectral profiles associated with the shortest time constant are similar for the two systems and resemble

the dG TAS at 4 ps (Figure 8c). Despite the similarity of the two DAS, the corresponding time constants differ significantly: 2.7 ps for GA and 4.5 ps, which is much higher, for AG. This difference in the dynamics can also be directly observed in changes in the TAS profiles recorded for the two dinucleotides (Figures 3 and 4 in reference [29]); the relative intensity of long and short wavelength peaks is inverted faster for GA compared to AG. We note that the longest time constants reported in the literature for the guanine chromophore range from 1.9 to 2.7 ps [31,50–52].



**Figure 8.** DAS derived from global fits of the TAS of AG (dashed lines, (a)) and GA (solid lines, (b)) between 4 and 45 ps. Red: DAS associated with the longer lifetime, 112 ps for AG and 170 ps for GA; green: DAS associated with the shorter lifetime, 4.5 ps for AG and 2.7 ps for GA; solid black line in (c): TAS obtained for dG alone at 4 ps; dotted line in (d): absorption spectrum corresponding to an equimolar mixture of the adenosine radical anion [53] and the guanine radical cation [54]. The TAS in (c) are normalized at their maximum intensity and in (d) at 520 nm.

The DAS associated with the longest time constants (Figure 8d) both exhibit peaks at ~384 nm and broad bands above 500 nm. A peak at 520 nm is present in the spectrum of an equimolar mixture of the guanine radical cation and the adenosine radical anion (Figure 8d), which are determined, respectively, using ns TA and pulsed radiolysis [53,54]. It is not surprising that the latter does not fully overlap with the TAS of the CT states, for which the transferred charge is not complete: it is: 0.4 a.u. for *anti-syn* AG and 0.7 a.u. for *anti-anti* GA, according to our computations. The TAS computed for the min-CT of the two systems, presented in Figure 9a,b, respectively, also exhibit one peak in the UV and a second above 500 nm. Moreover, it is blue-shifted with respect to that of the corresponding Franck–Condon state.



**Figure 9.** Comparison of computed TAS: (a) min-CT of *anti-syn* AG (dark blue line) and min- $\pi\pi^*$ A of *anti-anti* AG (cyan dashed line); (b) min-CT of *anti-anti* GA:  $S_2$  Franck–Condon state (dashed line) evolving toward the min-CT (solid line).

Unlike min- $\pi\pi^*$ G(La) and min-CT, it is difficult to obtain experimental information on the TAS of min- $\pi\pi^*$ A. Temps and coll. attributed a time constant of 0.45 ps to  $\pi\pi^*$ A, which was derived from global fits with two exponential functions [55]; the same time constant has been also reported by Kwok and coll. [56]. In both studies, the presented TAS peak at wavelengths shorter than 310 nm. Later experiments, which were performed with lower excitation intensity and higher time resolution, reported a transient species peaking at 380 nm and characterized by a lifetime of  $1.4 \pm 0.2$  ps instead [57]. In view of these discrepancies, the TAS computed for min- $\pi\pi^*$ A in the dinucleotides are precious. That of the minor conformer *anti-anti* AG is shown in Figure 9a; it exhibits a rich structure over the visible domain, with an intense band in the red part located at longer wavelengths compared to those of the min-CT of *anti-syn* AG.

## 4. Discussion

### 4.1. Base Stacking and Photon Absorption

An early work that pioneered the study of CT states in dinucleotides proposed a model, according to which they should be formed only between pre-stacked nucleobases, with the remaining excitations (75% in the case of AG) decaying as monomer bright states [34]. Therefore, a key question in the present study is whether the nucleobases are already stacked in the ground state and to what extent. Although it is not possible to obtain a quantitative answer, our results provide important qualitative information.

The hyperchromic and hypochromic effects detected in the thermal spectra (Figure 2b) are characteristic of chromophore stacking. They result from the coupling between  $\pi\pi^*$  and CT states [15,58], requiring orbital overlap. Most importantly, the sharp contrast observed between the dinucleotide TAS and those of an equivalent mixture of mononucleotides recorded below 100 fs (Figure 4a–c) demonstrates that the percentage of non-coupled chromophores in AG and GA is low.

The relative ground state energies computed for the various conformers with stacked nucleobases (Figure 5) suggest that, while only the *anti-anti* conformer is expected to be present in GA room temperature solutions, the situation is more complex for AG. For the latter, in addition to the most stable *anti-syn* conformer, the presence of a small amount of the *anti-anti* conformer is also possible. This is in agreement with the picture emerging from the CD spectra. As previously noted, the experimental CD spectrum of AG, unlike that of GA, exhibits multiple fluctuations above 220 nm (Figure 3a). This is readily explained by the coexistence of a major (*anti-syn*) and a minor (*anti-anti*) conformer, whose computed CD spectra are characterized by opposite patterns (Figure 3c); given that the signatures of the two AG conformers are not canceled out in the experimental CD spectra and only fluctuations are observed, the *anti-anti* AG concentration in the solutions is significantly smaller compared to that of *anti-syn* AG.

It is also worth noting that the peaks of the steady state computed for the major and minor **AG** conformers are located at shorter wavelengths, and their intensity is higher compared to that of *anti-anti* **GA** (Figure 6a). They follow a tendency similar to that of the experimental spectra (Figure 2a) but are significantly amplified. This suggests that although the comparison between computed and experimental spectra in the present study is not intended to be quantitative, the spectra of different systems computed following the same methodology reveal interesting trends.

#### 4.2. Relaxation Dynamics: From the Franck–Condon States to the Minima

A quantitative analysis of the spectra in Figure 4a,b is not possible due to three reasons. The first is the existence of several Franck–Condon states per conformer evolving toward different minima. The second is the lack of theoretical information regarding the dynamic patterns followed in this evolution. The third is the existence in **AG** of a minor conformer with an unknown concentration. However, we can make qualitative observations, assuming that the dominant structures are *anti-syn* for **AG** and *anti-anti* for **GA**, as determined theoretically, while for the former system, a smaller contribution from the *anti-anti* conformer is also possible.

The important changes observed in the *TAS* presented in Figure 4a,b are associated with the evolution along the various PES. This is supported by the rise of the *TA* signals in Figure 4d; while that of the monomers stops just after the end of the exciting laser pulse, in the case of the dinucleotides, it lasts longer. The fact that the maximum value is reached faster for **GA** compared to the **AG** (110 fs vs. 130 fs) could be due to an equilibrium between two conformers.

Although we cannot rule out that the relaxation process has already started before the end of the laser pulse, the *TAS* at 30 fs (Figure 7d) are likely to be dominated by the Franck–Condon states. The stronger intensity observed for **GA** is indeed reproduced in the *TAS* computed for the most stable conformers of the two dinucleotides (Figure 7c), taking into account the probability of each Franck–Condon to be populated by the exciting laser pulse (Figure 6).

Next, we search in the *TAS* evolution the fingerprints of the minima predicted theoretically: *sy*:  $\text{min-}\pi\pi^*\text{G}(\text{L}_a)$ , *min-CT*, and  $\text{min-}\pi\pi^*\text{A}$ . The global analysis performed on the experimental *TAS* recorded from 4 to 45 ps confirmed that  $\text{min-}\pi\pi^*\text{G}(\text{L}_a)$  and *min-CT* are indeed populated in both **AG** and **GA** (Figure 8). The early time dynamics (Figure 4) show that this population is very fast.

Starting from the simpler case of **GA**, for which a single conformer is dominant, we observe that, in parallel with the intensity increase, the band initially peaking around 620 nm progressively shifts to shorter wavelengths, reaching 580 nm at 100 fs (Figure 4b). We assign these changes to the evolution along the PES, leading from  $S_1$  and  $S_2$  to *min-CT*. According to the computed *TAS* (Figure 9b), the population of *min-CT* is manifested indeed by an increase in intensity and a blue shift compared to the corresponding Franck–Condon state. Consequently, we deduce that the changes observed in the long-wavelength band in Figure 4b reflect the dynamics of the charge transfer process.

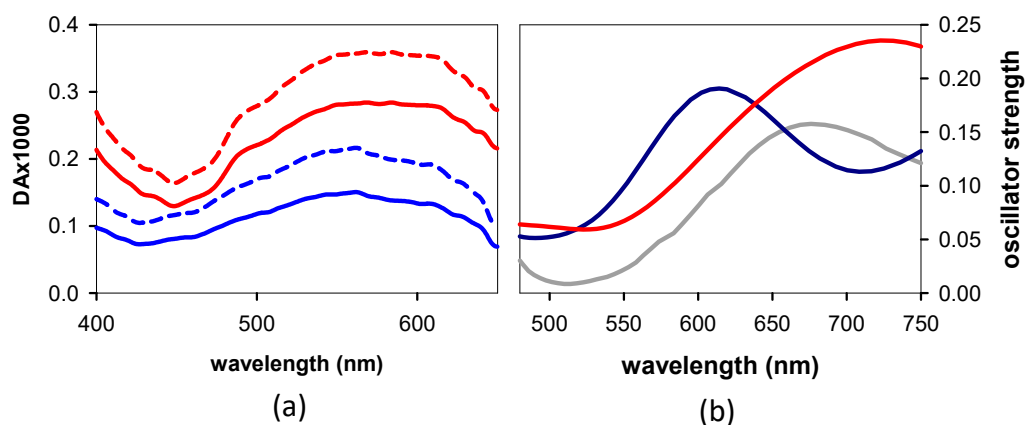
An important difference between the *TAS* of the two systems is that the long-wavelength band, shifting to shorter wavelengths for **GA**, progressively splits into two components for **AG**; at 100 fs, a peak at 586 nm and a shoulder at ~530 nm can be distinguished. Such a complex behavior is assigned to the population of  $\text{min-}\pi\pi^*\text{A}$  in the minor *anti-anti* **AG** conformer. Our interpretation is based on the computed *TAS*; the low-energy band observed in that of  $\text{min-}\pi\pi^*\text{A}$  is red-shifted compared to that of the *min-CT* of *anti-syn* **AG** (Figure 9a). Thus, the concomitant population of these two minima should induce a spectral evolution similar to that observed in Figure 4a.

The peak at ~440 nm growing in the *TAS* of both **AG** and **GA** is correlated with the guanosine chromophore [31]. Several experimental studies reported that the excited state relaxation of this chromophore in solution is very complex [50–52,59,60]. Moreover, a theoretical work that was performed combining quantum chemistry calculations and

molecular dynamics simulations identified the presence of three different minima in the PES of its first singlet excited state [61]. The first minimum absorbs at longer wavelengths (around 400 nm) than the third one, which is characterized by the longest lifetime. The latter was indeed detected through our global analysis (Figure 8c).

#### 4.3. Quantum Yields

In our previous publication, we reported on the relative  $\Phi_{CT}$  values; the value for **GA** was found to be 75% higher than that for **AG** [29]. This conclusion was drawn from the relative intensities of the UV bands present in the *TAS* at zero time, which were obtained from the *TAS* at 15 ps according to the equation  $(DA)_0 = (DA)_{15ps} / \exp(-15ps/\tau_{CT})$ . In the present more refined study, we examine this issue again. Now, we start from the *TAS* at 40 ps and focus on the low-energy band, which has been associated with the sum of the absorption spectra of the dA radical anion and the dG radical cation (Figure 8d). Applying the same formula as before, we find that the peak intensity is 71% higher for **GA** than for **AG** (Figure 10a). Then, using the molar absorption coefficient corresponding to an equimolar mixture of the dA radical anion [53] and the dG radical cation [54] ( $1230 \text{ mol}^{-1} \text{ Lcm}^{-1}$ ) and considering the concentration of absorbed photons ( $8 \times 10^{-6} \text{ molL}^{-1}$ ), we obtain a  $\Phi_{CT}$  value of 0.18 for **AG** and 0.32 for **GA**. According to our calculations, the oscillator strength of the low-energy peaks present in the *TAS* of the min-CT is higher than that corresponding to the sum of the absorption spectra computed for the dA radical anion and the dG radical cation (Figure 10b), suggesting that the determined values represent upper limits for the  $\Phi_{CT}$ .



**Figure 10.** Low-energy band of the CT states. (a) *TAS* recorded for **AG** (blue) and **GA** (red) at 40 ps (solid lines) and extrapolated to zero time (dashed lines). (b) *TAS* computed for the CT-min of *anti-syn* **AG** (dark blue) and *anti-anti* **GA** (red); the gray line corresponds to the sum of the spectra computed for the dA radical anion and the dG radical cation (average for the *anti* and *syn* conformations for each radical).

## 5. Conclusions

Our present theoretical and experimental study on the **AG** and **GA** dinucleotides, which is the continuation of our previous work on these systems [29], sheds important light on the excited state relaxation occurring in these systems upon excitation at 266 nm. Based on a series of quantum chemistry calculations, combined with broad-band transient absorption spectroscopy at the exceptional resolution of 30 fs, we followed the processes occurring at early times, from photon absorption to the population of the CT states.

The main findings are summarized as follows:

- Our computations on these systems showed that the stacking pattern corresponding to the most stable geometry of the studied systems depends on the dinucleotide polarity; while the *anti-anti* conformation present in B-form duplexes is adopted in **GA**, **AG** corresponds to the *anti-syn* configuration.



- The computed Franck–Condon states and their evolution depend both on the polarity and the stacking geometry.
- The excited state minima predicted theoretically, min-CT, min- $\pi\pi^*$ G(La), and min- $\pi\pi^*$ A, were detected in the experimental TAS; they are reached within ~120 fs.
- From the experimental TAS, we deduced that the largest portion of the nucleobases within the dinucleotides are electronically coupled in their ground state. This does not preclude the existence of a minimum localized on a single nucleobase, min- $\pi\pi^*$ G(La), whose lifetime depends on the dinucleotide polarity.
- As a result of the competition among the different relaxation paths, the quantum yields determined for the formation of the CT state are relatively low. The estimated upper values in AG and GA are 0.18 and 0.32, respectively.
- From a methodological point of view, our computations showed that the TAS of the various excited states involved in the relaxation process exhibit different spectral shapes and oscillator strengths. This reason renders the use of the pre-exponential factors derived from fits of the TA signals inappropriate for the determination of their populations.

The knowledge acquired by the present study on dinucleotides will serve as a foundation for the characterization of the abovementioned processes in G-quadruplexes, with adenines at the 3' and/or the 5' ends, whose  $\Phi_1$  values at 266 nm are the highest determined for any DNA system [27].

**Supplementary Materials:** The following supporting information can be downloaded at <https://www.mdpi.com/article/10.3390/biom14121548/s1>: figures with experimental results; tables with computational results.

**Author Contributions:** Conceptualization: L.M.-F., G.C. and D.M.; data curation: V.P. and L.M.-F.; formal analysis: V.P., L.M.-F., E.B. and D.M.; funding acquisition: L.M.-F., G.C., M.M. and D.M.; investigation: V.P., L.M.-F. and L.U.; methodology: L.M.-F., G.C. and M.M.; supervision: G.C. and M.M.; validation: all authors; visualization: V.P., L.M.-F., E.B. and D.M.; writing—original draft: V.P., L.M.-F. and D.M.; writing—review and editing: V.P., L.M.-F., G.C., E.B. and D.M. All authors have read and agreed to the published version of the manuscript.

**Funding:** This work has received funding from the European Union's Horizon 2020 research and innovation program under the Marie Skłodowska-Curie ITN program (grant No. 765266—LightDyNAMics and grant No. 812992—MUSIQ). G.C. acknowledges financial support by the European Union's NextGenerationEU Programme with the I-PHOQS Infrastructure [IR0000016, ID D2B8D520, CUP B53C22001750006] "Integrated infrastructure initiative in Photonic and Quantum Sciences". This research project was made possible through the access granted by the Galician Supercomputing Center (CESGA) to its supercomputing infrastructure. The supercomputer FinisTerae III and its permanent data storage system have been funded by the Spanish Ministry of Science and Innovation, the Galician Government, and the European Regional Development Fund (ERDF).

**Institutional Review Board Statement:** Not applicable.

**Informed Consent Statement:** Not applicable.

**Data Availability Statement:** The original contributions presented in the study are included in the article/Supplementary Materials, further inquiries can be directed to the corresponding authors.

**Conflicts of Interest:** The authors declare no conflicts of interest.

## References

1. Becker, D.; Kumar, A.; Adhikary, A.; Sevilla, M.D. Gamma- and ion-beam DNA radiation damage: Theory and experiment. In *DNA Damage, DNA Repair and Disease*; Dizdaroglu, M., Stephen Lloyd, R., Eds.; Chemical Biology; RSC: Cambridge, UK, 2021; Volume 2, pp. 426–457.
2. Candeias, L.P.; Steenken, S. Structure and acid-base properties of one-electron-oxidized deoxyguanosine, guanosine, and 1-methylguanosine. *J. Am. Chem. Soc.* **1989**, *111*, 1094–1099. [[CrossRef](#)]

3. O'Neill, P.; Parker, A.W.; Plumb, M.A.; Siebbeles, L.D.A. Guanine modifications following ionization of DNA occurs predominantly via intra- and not interstrand charge migration: An experimental and theoretical study. *J. Phys. Chem. B* **2001**, *105*, 5283–5290.
4. Melvin, T.; Plumb, M.A.; Botchway, S.W.; Oneill, P.; Parker, A.W. 193 nm Light Induces Single-strand Breakage of DNA Predominantly at Guanine. *Photochem. Photobiol.* **1995**, *61*, 584–591. [[CrossRef](#)]
5. Balanikas, E.; Banyasz, A.; Douki, T.; Baldacchino, G.; Markovitsi, D. Guanine Radicals Induced in DNA by Low-Energy Photoionization. *Acc. Chem. Res.* **2020**, *53*, 1511–1519. [[CrossRef](#)]
6. Kawai, K.; Fujitsuka, M.; Majima, T. Selective guanine oxidation by UVB-irradiation in telomeric DNA. *Chem. Commun.* **2005**, 1476–1477. [[CrossRef](#)] [[PubMed](#)]
7. Balanikas, E.; Markovitsi, D. DNA photoionization: From high to low energies. In *DNA Photodamage: From Light Absorption to Cellular Responses and Skin Cancer*; Improta, R., Douki, T., Eds.; Comprehensive Series in Photochemical and Photobiological Science; RSC: Cambridge, UK, 2021; pp. 37–54.
8. Candeias, L.P.; Oneill, P.; Jones, G.D.D.; Steenken, S. Ionization of polynucleotides and DNA in aqueous solution by 193 nm pulsed laser light—Identification of base-derived radicals. *Int. J. Radiat. Biol.* **1992**, *61*, 15–20. [[CrossRef](#)]
9. Douki, T. Effect of denaturation on the photochemistry of pyrimidine bases in isolated DNA. *J. Photochem. Photobiol B* **2006**, *82*, 45–52. [[CrossRef](#)]
10. Mouret, S.; Baudouin, C.; Charveron, M.; Favier, A.; Cadet, J.; Douki, T. Cyclobutane pyrimidine dimers are predominant DNA lesions in whole human skin exposed to UVA radiation. *Proc. Natl. Acad. Sci. USA* **2006**, *103*, 13765–13770. [[CrossRef](#)]
11. Schroeder, C.A.; Pluharova, E.; Seidel, R.; Schroeder, W.P.; Faubel, M.; Slavicek, P.; Winter, B.; Jungwirth, P.; Bradforth, S.E. Oxidation Half-Reaction of Aqueous Nucleosides and Nucleotides via Photoelectron Spectroscopy Augmented by ab Initio Calculations. *J. Am. Chem. Soc.* **2015**, *137*, 201–209. [[CrossRef](#)]
12. Pluharova, E.; Schroeder, C.; Seidel, R.; Bradforth, S.E.; Winter, B.; Faubel, M.; Slavicek, P.; Jungwirth, P. Unexpectedly Small Effect of the DNA Environment on Vertical Ionization Energies of Aqueous Nucleobases. *J. Phys. Chem. Lett.* **2013**, *4*, 3766–3769. [[CrossRef](#)]
13. Pluharova, E.; Slavicek, P.; Jungwirth, P. Modeling Photoionization of Aqueous DNA and Its Components. *Acc. Chem. Res.* **2015**, *48*, 1209–1217. [[CrossRef](#)]
14. Nogueira, J.J.; Plasser, F.; Gonzalez, L. Electronic delocalization, charge transfer and hypochromism in the UV absorption spectrum of polyadenine unravelled by multiscale computations and quantitative wavefunction analysis. *Chem. Sci.* **2017**, *8*, 5682–5691. [[CrossRef](#)] [[PubMed](#)]
15. Plasser, F.; Aquino, A.; Lischka, H.; Nachtigallova, D. Electronic Excitation Processes in Single-Strand and Double-Strand DNA: A Computational Approach. *Top. Curr. Chem.* **2015**, *356*, 1–38. [[PubMed](#)]
16. Spata, V.A.; Matsika, S. Role of Excitonic Coupling and Charge-Transfer States in the Absorption and CD Spectra of Adenine-Based Oligonucleotides Investigated through QM/MM Simulations. *J. Phys. Chem. A* **2014**, *118*, 12021–12030. [[CrossRef](#)] [[PubMed](#)]
17. Santoro, F.; Improta, R.; Avila, F.; Segado, M.; Lami, A. The interplay between neutral exciton and charge transfer states in single-strand polyadenine: A quantum dynamical investigation. *Photochem. Photobiol. Sci.* **2013**, *12*, 1527–1543. [[CrossRef](#)] [[PubMed](#)]
18. Aquino, A.J.A.; Nachtigallova, D.; Hobza, P.; Truhlar, D.G.; Hattig, C.; Lischka, H. The Charge-Transfer States in a Stacked Nucleobase Dimer Complex: A Benchmark Study. *J. Comput. Chem.* **2011**, *32*, 1217–1227. [[CrossRef](#)] [[PubMed](#)]
19. Blancafort, L.; Voityuk, A.A. Exciton delocalization, charge transfer, and electronic coupling for singlet excitation energy transfer between stacked nucleobases in DNA: An MS-CASPT2 study. *J. Chem. Phys.* **2014**, *140*, 095102. [[CrossRef](#)] [[PubMed](#)]
20. Improta, R.; Santoro, F.; Blancafort, L. Quantum Mechanical Studies on the Photophysics and the Photochemistry of Nucleic Acids and Nucleobases. *Chem. Rev.* **2016**, *116*, 3540–3593. [[CrossRef](#)]
21. Chen, J.; Zhang, Y.; Kohler, B. Excited states in DNA strands investigated by ultrafast laser spectroscopy. *Top. Curr. Chem.* **2015**, *356*, 39–87.
22. Schreier, W.J.; Gilch, P.; Zinth, W. Early Events of DNA Photodamage. *Annu. Rev. Phys. Chem.* **2015**, *66*, 497–519. [[CrossRef](#)]
23. Kwok, W.M.; Ma, C.S.; Phillips, D.L. “Bright” and “Dark” excited states of an alternating AT oligomer characterized by femtosecond broadband spectroscopy. *J. Phys. Chem. B* **2009**, *113*, 11527–11534. [[CrossRef](#)] [[PubMed](#)]
24. Bucher, D.B.; Pilles, B.M.; Carell, T.; Zinth, W. Charge separation and charge delocalization identified in long-living states of photoexcited DNA. *Proc. Natl. Acad. Sci. USA* **2014**, *111*, 4369–4374. [[CrossRef](#)]
25. Kufner, C.L.; Crucilla, S.; Ding, D.; Stadlbauer, P.; Sponer, J.; Szostak, J.W.; Sasselov, D.D.; Szabla, R. Photoinduced charge separation and DNA self-repair depend on sequence directionality and stacking pattern. *Chem. Sci.* **2023**, *15*, 2158–2166. [[CrossRef](#)]
26. Schiedt, J.; Weinkauff, R.; Neumark, D.M.; Schlag, E.W. Anion spectroscopy of uracil, thymine and the amino-oxo and amino-hydroxy tautomers of cytosine and their water clusters. *Chem. Phys.* **1998**, *239*, 511–524. [[CrossRef](#)]
27. Balanikas, E.; Martinez-Fernandez, L.; Improta, R.; Podbevsek, P.; Baldacchino, G.; Markovitsi, D. The Structural Duality of Nucleobases in Guanine Quadruplexes Controls Their Low-Energy Photoionization. *J. Phys. Chem. Lett.* **2021**, *12*, 8309–8313. [[CrossRef](#)] [[PubMed](#)]
28. Palecek, E.; Bartosik, M. Electrochemistry of Nucleic Acids. *Chem. Rev.* **2012**, *112*, 3427–3481. [[CrossRef](#)]

29. Petropoulos, V.; Uboldi, L.; Maiuri, M.; Cerullo, G.; Martinez-Fernandez, L.; Balanikas, E.; Markovitsi, D. Effect of the DNA polarity on the relaxation of its electronic excited states. *J. Phys. Chem. Lett.* **2023**, *14*, 10219–10224. [[CrossRef](#)]
30. Duchi, M.; O'Hagan, M.P.; Kumar, R.; Bennie, S.J.; Galan, M.C.; Curchod, B.F.E.; Oliver, T.A.A. Exploring ultraviolet photoinduced charge-transfer dynamics in a model dinucleotide of guanine and thymine. *Phys. Chem. Chem. Phys.* **2019**, *21*, 14407–14417. [[CrossRef](#)] [[PubMed](#)]
31. Petropoulos, V.; Martinez-Fernandez, L.; Uboldi, L.; Maiuri, M.; Cerullo, G.; Balanikas, E.; Markovitsi, D. Real-time observation of sub-100-fs charge and energy transfer processes in DNA dinucleotides. *Chem. Sci.* **2024**, *15*, 12098–12107. [[CrossRef](#)]
32. Ma, C.S.; Chan, R.C.-T.; Chan, C.T.-L.; Wong, A.K.-W.; Kwok, W.-M. Real-time Monitoring Excitation Dynamics of Human Telomeric Guanine Quadruplexes: Effect of Folding Topology, Metal Cation, and Confinement by Nanocavity Water Pool. *J. Phys. Chem. Lett.* **2019**, *10*, 7577–7585. [[CrossRef](#)]
33. Martinez-Fernandez, L.; Changuenet, P.; Banyasz, A.; Gustavsson, T.; Markovitsi, D.; Improta, R. A Comprehensive Study of Guanine Excited State Relaxation and Photoreactivity in G-Quadruplexes. *J. Phys. Chem. Lett.* **2019**, *10*, 6873–6877. [[CrossRef](#)]
34. Takaya, T.; Su, C.; de La Harpe, K.; Crespo-Hernandez, C.E.; Kohler, B. UV excitation of single DNA and RNA strands produces high yields of exciplex states between two stacked bases. *Proc. Natl. Acad. Sci. USA* **2008**, *105*, 10285–10290. [[CrossRef](#)]
35. Stuhldreier, M.C.; Temps, F. Ultrafast photo-initiated molecular quantum dynamics in the DNA dinucleotide d(ApG) revealed by broadband transient absorption spectroscopy. *Faraday Disc.* **2013**, *163*, 173–188. [[CrossRef](#)]
36. Martínez-Fernández, L.; Green, J.A.; Esposito, L.; Jouybari, M.Y.; Zhang, Y.Y.; Santoro, F.; Kohler, B.; Improta, R. The photoactivated dynamics of dGpdC and dCpdG sequences in DNA: A comprehensive quantum mechanical study. *Chem. Sci.* **2024**, *15*, 9676–9693. [[CrossRef](#)]
37. Kufner, C.L.; Zinth, W.; Bucher, D.B. UV-Induced Charge-Transfer States in Short Guanosine-Containing DNA Oligonucleotides. *ChemBioChem* **2020**, *21*, 2306–2310. [[CrossRef](#)] [[PubMed](#)]
38. Black, P.J.; Bernhard, W.A. EPR Detection of an Electron Scavenging Contaminant in Irradiated Deoxyoligonucleotides: One-Electron Reduced Benzoyl. *J. Phys. Chem. B* **2011**, *115*, 8009–8013. [[CrossRef](#)] [[PubMed](#)]
39. Baldassarri, E.; Orto, M.G.; Spinozzi, F.; Round, A.; Ferrero, C.; Mariani, P. K<sup>+</sup> vs. Na<sup>+</sup> Effects on the Self-Assembly of Guanosine 5'-Monophosphate: A Solution SAXS Structural Study. *Nanomaterials* **2020**, *10*, 629. [[CrossRef](#)] [[PubMed](#)]
40. Borrego-Varillas, R.; Ganzer, L.; Cerullo, G.; Manzoni, C. Ultraviolet Transient Absorption Spectrometer with Sub-20-fs Time Resolution. *Appl. Sci.* **2018**, *8*, 989. [[CrossRef](#)]
41. Zhao, Y.; Schultz, N.E.; Truhlar, D.G. Design of density functionals by combining the method of constraint satisfaction with parametrization for thermochemistry, thermochemical kinetics, and noncovalent interactions. *J. Chem. Theory Comput.* **2006**, *2*, 364–382. [[CrossRef](#)]
42. Zhao, Y.; Truhlar, D.G. Density functionals with broad applicability in chemistry. *Acc. Chem. Res.* **2008**, *41*, 157–167. [[CrossRef](#)]
43. Tomasi, J.; Mennucci, B.; Cammi, R. Quantum mechanical continuum solvation models. *Chem. Rev.* **2005**, *105*, 2999–3093. [[CrossRef](#)] [[PubMed](#)]
44. Martinez-Fernandez, L.; Esposito, L.; Improta, R. Studying the excited electronic states of guanine rich DNA quadruplexes by quantum mechanical methods: Main achievements and perspectives. *Photochem. Photobiol. Sci.* **2020**, *19*, 436–444. [[CrossRef](#)]
45. Martinez-Fernandez, L.; Santoro, F.; Improta, R. Nucleic Acids as a Playground for the Computational Study of the Photophysics and Photochemistry of Multichromophore Assemblies. *Acc. Chem. Res.* **2022**, *55*, 2077–2087. [[CrossRef](#)]
46. Frisch, M.J.; Trucks, G.W.; Schlegel, H.B.; Scuseria, G.E.; Robb, M.A.; Cheeseman, J.R.; Scalmani, G.; Barone, V.; Petersson, G.A.; Nakatsuji, H.; et al. *Gaussian 16 Rev. C.01*; Gaussian Inc.: Wallingford, CT, USA, 2016.
47. Ferrer, F.J.A.; Cerezo, J.; Stendardo, E.; Improta, R.; Santoro, F. Insights for an Accurate Comparison of Computational Data to Experimental Absorption and Emission Spectra: Beyond the Vertical Transition Approximation. *J. Chem. Theory Comput.* **2013**, *9*, 2072–2082. [[CrossRef](#)] [[PubMed](#)]
48. Bouvier, B.; Gustavsson, T.; Markovitsi, D.; Millié, P. Dipolar coupling between electronic transitions of the DNA bases and its relevance to exciton states in double helices. *Chem. Phys.* **2002**, *275*, 75–92. [[CrossRef](#)]
49. Lu, T.; Chen, F.W. Multiwfn: A multifunctional wavefunction analyzer. *J. Comput. Chem.* **2012**, *33*, 580–592. [[CrossRef](#)]
50. Karunakaran, V.; Kleinermanns, K.; Improta, R.; Kovalenko, S.A. Photoinduced dynamics of guanosine monophosphate in water from broad-band transient absorption spectroscopy and quantum-chemical calculations. *J. Am. Chem. Soc.* **2009**, *131*, 5839–5850. [[CrossRef](#)] [[PubMed](#)]
51. Krul, S.E.; Hoehn, S.J.; Feierabend, K.J.; Crespo-Hernández, C.E. Excited state dynamics of 7-deazaguanosine and guanosine 5'-monophosphate. *J. Chem. Phys.* **2021**, *154*, 075103. [[CrossRef](#)]
52. Wang, D.H.; Wang, X.L.; Jiang, Y.R.; Cao, S.M.; Jin, P.P.; Pan, H.F.; Sun, H.T.; Sun, Z.R.; Chen, J.Q. Excited State Dynamics of Methylated Guanosine Derivatives Revealed by Femtosecond Time-resolved Spectroscopy. *Photochem. Photobiol.* **2022**, *98*, 1008–1016. [[CrossRef](#)]
53. Candeias, L.P.; Steenken, S. Electron adducts of adenine nucleosides and nucleotides in aqueous solution: Protonation at two carbon sites (C2 and C8) and Intra- and intermolecular catalysis by phosphate. *J. Phys. Chem.* **1992**, *96*, 937–944. [[CrossRef](#)]
54. Candeias, L.P.; Steenken, S. Ionization of purine nucleosides and nucleotides and their components by 193-nm laser photolysis in aqueous solution: Model studies for oxidative damage of DNA. *J. Am. Chem. Soc.* **1992**, *114*, 699–704. [[CrossRef](#)]
55. Stange, U.C.; Temps, F. Ultrafast electronic deactivation of UV-excited adenine and its ribo- and deoxyribonucleosides and -nucleotides: A comparative study. *Chem. Phys.* **2018**, *515*, 441–451. [[CrossRef](#)]

56. Kwok, W.-M.; Ma, C.; Phillips, D.L. Femtosecond time- and wavelength-resolved fluorescence and absorption study of the excited states of adenosine and an adenine oligomer. *J. Am. Chem. Soc.* **2006**, *128*, 11894–11905. [[CrossRef](#)] [[PubMed](#)]
57. Borrego-Varillas, R.; Cerullo, G.; Markovitsi, D. Exciton Trapping Dynamics in DNA Multimers. *J. Phys. Chem. Lett.* **2019**, *10*, 1639–1643. [[CrossRef](#)] [[PubMed](#)]
58. Varsano, D.; Di Felice, R.; Marques, M.A.L.; Rubio, A. A TDDFT study of the excited states of DNA bases and their assemblies. *J. Phys. Chem. B* **2006**, *110*, 7129–7138. [[CrossRef](#)]
59. Miannay, F.A.; Gustavsson, T.; Banyasz, A.; Markovitsi, D. Excited state dynamics of dGMP measured by steady-state and femtosecond fluorescence spectroscopy. *J. Phys. Chem. A* **2010**, *114*, 3256–3263. [[CrossRef](#)]
60. Cheng, C.C.-W.; Ma, C.; Chan, C.T.-L.; Ho, K.Y.-F.; Kwok, W.-M. The solvent effect and identification of a weakly emissive state in nonradiative dynamics of guanine nucleosides and nucleotides—A combined femtosecond broadband time-resolved fluorescence and transient absorption study. *Photochem. Photobiol. Sci.* **2013**, *12*, 1351–1365. [[CrossRef](#)]
61. Ortín-Fernández, J.; González-Vázquez, J.; Martínez-Fernández, L.; Corral, I. Molecular Identification of the Transient Species Mediating the Deactivation Dynamics of Solvated Guanosine and Deazaguanosine. *Molecules* **2022**, *27*, 989. [[CrossRef](#)]

**Disclaimer/Publisher’s Note:** The statements, opinions and data contained in all publications are solely those of the individual author(s) and contributor(s) and not of MDPI and/or the editor(s). MDPI and/or the editor(s) disclaim responsibility for any injury to people or property resulting from any ideas, methods, instructions or products referred to in the content.